Research Square

Preprints are preliminary reports that have not undergone peer review.
They should not be considered conclusive, used to inform clinical practice,
or referenced by the media as validated information.

CHES1/RORA axis modulated the progression of triple-negative breast cancer by tuning PI3K/AKT signaling pathway

Pengfei Wei

pfwei@mail.ustc.edu.cn

Shandong Medical and Pharmaceutical University https://orcid.org/0000-0002-5786-6580

Yujie Wang

Shandong Medical and Pharmaceutical University

Zhaowei Xu

Demin Kong

Yong Mei

Yuxue Xu

Xiaojie Tang

Guilong Zhang

Yangyang Yang

Article

Keywords: Triple-negative breast cancer, CHES1 (FOXN3), RORA, PI3K/AKT signaling, Transcriptional repression, tumorigenesis

Posted Date: October 12th, 2026

DOI: https://doi.org/10.21203/rs.3.rs-10952681/v1

License: This work is licensed under a Creative Commons Attribution 4.0 International License.
Read Full License

Additional Declarations: There is **NO** conflict of interest to disclose.

CHES1/RORA axis modulated the progression of triple-negative breast cancer by tuning PI3K/AKT signaling pathway

Yujie Wang[1, †], Zhaowei Xu[1, †], Demin Kong[1], Yong Mei[2], Yuxue Xu[1], Xiaojie Tang[3], Guilong Zhang[1, *], Pengfei Wei[1, *], Yangyang Yang[4, *]

[1] Shandong Center of Technology Innovation for Molecular Targeting and Intelligent Diagnosis and Treatment, Shandong Key Lab of Complex Medical Intelligence and Aging, School of Pharmacy, Yantai Key Laboratory of Tumor Metabolism and Traditional Chinese Medicine Pharmacology, Shandong Medical and Pharmaceutical University, Yantai, 264003, China.

[2] Department of Hepatobiliary Surgery, the Affiliated Hospital of Guizhou Medical University, Guiyi Street, Yunyan District, Guiyang, 550004, China.

[3] Department of Spinal Surgery, Yantai Affiliated Hospital of Shandong Medical and Pharmaceutical University, Yantai 264100, China

[4] School of Basic Medical Sciences, Shandong Medical and Pharmaceutical University, Yantai, 264003, China.

† These author contributed equally.

Corresponding authors：

Pengfei Wei, E-mail: pfwei@sdmpu.edu.cn.

Yangyang Yang, E-mail: yang0514@sdmpu.edu.cn

Guilong Zhang, E-mail: glzhang@sdmpu.edu.cn

Abstract

Circadian clock disruption is closely related with aggressive phenotype and therapeutic resistance of breast cancer. The clock gene retinoic acid-related orphan nuclear receptor α (*RORA*) exerts anti‑ tumor functions and is often silenced in breast cancer, yet the causes of its dysregulation are still unknown. We demonstrated that checkpoint suppressor 1 (CHES1) directly bond to the promoter of *RORA* and transcriptionally suppressed its expression, and CHES1 had negatively expression correlation with RORA in TNBC. Functionally, RORA overexpression significantly repressed the proliferation and metastasis of triple-negative breast cancer (TNBC), whose inhibition partially rescued CHES1 knockdown-mediated tumor-suppressing effect in TNBC, indicating that RORA was the downstream effector of CHES1, and CHES1/RORA axis regulated the progression of TNBC. In addition, integrated analysis of transcriptome and function investigation revealed that PI3K/AKT signaling pathway was modulated by CHES1/RORA axis in TNBC, pharmaceutical activation or inhibition of PI3K/AKT blocked CHES1/RORA-mediated tumorigenesis. In conclusion, this study identified a novel transcription regulatory axis orchestrated oncogenic pathway in TNBC, which provided deep understanding for signaling networks and gave an avenue for therapeutic strategy of TNBC.

Keywords: Triple-negative breast cancer; CHES1 (FOXN3); RORA; PI3K/AKT signaling; Transcriptional repression; tumorigenesis

Introduction

Triple-negative breast cancer (TNBC) is pathologically characterized by the simultaneous absence of estrogen receptor (ER), human epidermal growth factor receptor 2 (HER2), and progesterone receptor (PR) [1]. This triple-negative phenotype renders endocrine therapy and anti-HER2 targeted agents completely ineffective, which constitutes the primary cause of therapeutic bottlenecks in clinical practice [2]. Distinct from other breast cancer subtypes, TNBC exhibits stronger proliferative, invasive, and metastatic capacities, accompanied by markedly elevated risks of early recurrence and lymph node metastasis, as well as persistently high long-term mortality. It remains a critical clinical challenge that urgently needs to be addressed in the field of female breast malignancies worldwide [3, 4]. Recently, poly adenosine diphosphate-ribose polymerase (PARP) inhibitors, antibody-drug conjugates and immune checkpoint inhibitors have been gradually applied to TNBC clinical management. Nevertheless, most patients fail to achieve durable long-term anti-tumor benefits [4]. The malignant progression and therapeutic resistance of TNBC are driven by multilayered molecular networks involving aberrant signaling crosstalk, tumor microenvironment interactions and extensive intratumoral heterogeneity. To date, the core regulatory hubs and dynamic underlying mechanisms have not been systematically elucidated[5, 6], and key functional molecules governing tumor progression remain largely unidentified, greatly hindering the development of novel targeted therapeutics. Accordingly, identifying driver molecules of TNBC and deciphering their full regulatory cascades bears significant translational value for breaking through current therapeutic limitations.

Checkpoint suppressor 1 (CHES1), also termed Forkhead box N3 (FOXN3), is a multifunctional transcriptional regulator belonging to the Forkhead box protein family. It participates in a broad spectrum of biological processes, including the maintenance of metabolic homeostasis [7], suppression of tissue fibrosis[8, 9], regulation of inflammatory responses [10], and vascular physiological remodeling [11]. The regulatory role of CHES1 in breast cancer exhibits profound subtype specificity. In ERα-positive luminal breast cancer, CHES1 directly interacts with ERα and recruits the NAD+-dependent deacetylase sirtuin 1 to repress acetylation-dependent ERα transcriptional activity, thereby blocking estrogen-driven tumor cell proliferation and exerting tumor-suppressive effects [12]. In stark contrast, CHES1 is markedly overexpressed in TNBC cells and tissues, and its protein abundance positively correlates with aggressive invasive/metastatic phenotypes and unfavorable patient prognosis [13]. Mechanistic investigations have validated that CHES1 undergoes reversible acetylation coordinated by the acetyltransferase p300 and deacetylase HDAC1. Acetylation antagonizes the ubiquitination of CHES1 and alleviates proteasome-mediated protein degradation, leading to aberrant accumulation of CHES1 within TNBC cells [13]. Current functional assays only demonstrate that abundant CHES1 transcriptionally activates proliferation- and invasion-related genes such as snail family transcriptional repressor 1, matrix metallopeptidase 9 and platelet-derived growth factor D to facilitate TNBC progression. [13]. Nevertheless, the complete transcriptional regulatory network governed by CHES1 during tumorigenesis remains largely uncharacterized.

Retinoic acid receptor-related orphan receptors (RORs) are multifunctional

transcription factors that exert essential roles in diverse biological processes including circadian rhythm regulation and tumorigenesis [14]. Clock disruption by jet lag or dysfunction of core genes is closely associated with aggressive phenotype and therapeutic resistance of breast cancer [15, 16]. As a core tumor-suppressive circadian clock molecule, RORA has been identified as a potential tumor suppressor [17, 18]. Accumulating evidence has validated the anti-tumor function of RORA in multiple malignancies, such as nasopharyngeal carcinoma [19, 20] and lung cancer [21]. In melanoma, RORA reinforces anti-tumor immune surveillance via repressing PD-L1 expression [22]. In breast cancer, RORA has been characterized as a tumor-suppressive nuclear receptor [17, 18]. Mechanistically, it restrains epithelial-mesenchymal transition (EMT) and malignant progression by transcriptionally repressing metastasis-associated genes or reducing intracellular ROS levels and suppressing the expression of ROS-triggered pro-inflammatory cytokines [23], rendering it a promising therapeutic candidate targeting inflammation and oxidative stress pathways in breast cancer. Genetic cohort studies have further revealed that the recessive mutation of the *RORA* rs4774388 polymorphism elevates the susceptibility to breast cancer [24]. One study focusing on nobiletin (NOB) in triple-negative breast cancer (TNBC) demonstrated that NOB exerts anti-cancer effects by activating ROR nuclear receptors to inhibit the NF-κB pathway, and can synergize with chemotherapeutic agents to strengthen therapeutic efficacy. Consistently, this work confirmed frequent downregulation of RORA in breast cancer, whereas RORA overexpression markedly represses cell proliferation and metastasis in TNBC [25]. Nevertheless, the upstream regulatory mechanisms accounting for RORA

dysregulation and its transcriptional repression in breast cancer remain largely unexplored.

Here, we demonstrated that CHES1 expression was inversely correlated with RORA in TNBC. Additionally, CHES1 could directly bind to the *RORA* promoter and transcriptionally repress its expression. Functionally, RORA attenuated TNBC cell proliferation, migration, and invasion of TNBC. Mechanical investigation revealed that the downstream effective pathway of the CHES1/RORA axis was PI3K/AKT, a canonical oncogenic pathway that is aberrant activated in TNBC [26, 27]. Interference or pharmaceutical inhibition on CHES1/RORA axis impaired the tumorigenesis and tuned the PI3K/AKT activation in TNBC. Taken together, these results identified the central circadian clock gene RORA was downstream effector of CHES1 and revealed a novel CHES1-RORA-PI3K/AKT regulatory axis contributed to tumorigenesis in TNBC.

Materials and Methods

Cell Culture and Reagents

MDA-MB-231, BT549, SUM159, MDA-MB-436 and HEK-293T cells were procured from accredited cell banks. MDA-MB-231, MDA-MB-436, and HEK-293T cells were maintained in high-glucose DMEM (Procell, PM150210), while SUM159 and BT549 cells were cultured in RPMI-1640 (Procell, PM150110), both media supplemented with 10% FBS (Vazyme, F101-03) and penicillin-streptomycin. Transfections were conducted using JetPrime (Polyplus, 114-15) in accordance with the manufacturer's instructions. All cell lines were authenticated by STR profiling and routinely screened for mycoplasma. T0901317 (TargetMol, T2008) and LY294002 (TargetMol, T6690)

were obtained from TargetMol Chemicals and dissolved in DMSO.

RNA Extraction, Reverse Transcription, and Quantitative Real-Time PCR (qRT-PCR)

TRIzol reagent (TaKaRa, 9108) was utilized to isolate total RNA from cultured cells, and cDNA was subsequently prepared from the extracted RNA by reverse transcription using PrimeScrip™ IV 1st Strand cDNA Synthesis Mix (TaKaRa, 6215). For quantitative gene expression analysis, we employed SYBR Green Master Mix (Vazyme, Q321-02) on an Applied Biosystems 7500 Fast Dx Real-Time PCR System. The qPCR program consisted of an initial denaturation at 95 °C for 10 min, followed by 36 amplification cycles of 95 °C for 25 s, 60 °C for 1 min, and 72 °C for 30 s. Expression levels were calculated by virtue of the $2^{\wedge(-\Delta\Delta Ct)}$ method and normalized to the housekeeping gene GAPDH. Primers were synthesized by Tsingke Biotechnology (Beijing, China) and the detailed information were listed below.

FOXN3:

5’-AAATGGAGCGCGGGTCCTGAG-3’ (Sense)

5’-GCAGCTGGTGATGCCATTCCT-3’ (Antisense)

RORA:

5’-CCTCAACAGACTGTGGCACCTAAAA-3’ (Sense)

5’ -CCTTTAAATATGGTCTTTTTTGGGC-3’ (Antisense)

BMAL1:

5’-GACCTACTCTCCGGTTCCCT-3’ (Sense)

5’ - GCATATTCTAACTGGTAGTCAGTGG -3’ (Antisense)

GAPDH:

5’-TCAAGTGGGGCGATGCTGGC-3’ (Sense)

5’ - TGGGGGCATCAGCAGAGGGG -3’ (Antisense)

RNA Sequencing and Bioinformatic Analysis

RNA sequencing was conducted by Shanghai OE Biotechnology on an Illumina Hiseq 6000 platform. Raw sequencing reads were filtered to obtain high-quality reads as follows: (1) removal of reads containing adapters; (2) removal of reads with non-AGCT bases at the 5' end; (3) trimming of low-quality read ends; (4) removal of reads with N content >10%; (5) discarding reads shorter than 25 bp. High-quality reads were aligned to the reference genome using HISAT2, followed by quantitative analysis using StringTie. Differential expression analysis was performed using DESeq2, with genes with $P<0.05$ and $|Log_2FC|>1$ defined as differentially expressed genes. CHES1 binding motifs and potential binding sites upstream of the RORA transcription start site were analyzed and downloaded from the JASPAR database (https://jaspar.genereg.net/). Heatmaps, Venn diagrams, and GO and Kyoto Encyclopedia of Genes and Genomes (KEGG) enrichment analyses of RNA-seq data were performed using a Bioinformatics Platform (https://www.bioinformatics.com.cn/), a comprehensive and user-friendly biomedical data visualization tool.

Western Blotting

Cellular proteins were isolated using RIPA lysis buffer (Beyotime, P0013) supplemented with a protease inhibitor cocktail (Bimake, B15001) and maintained on ice throughout the extraction procedure. Insoluble debris was removed by

centrifugation, and the resulting lysates were subjected to protein quantification with a BCA kit (Beyotime, P0012). Samples were then boiled in SDS-containing loading buffer (Meilun, MA0479-2), electrophoretically separated on polyacrylamide gels, and transferred electrophoretically to PVDF membranes (Millipore, IPVH00010). Non-specific binding sites were blocked with 5% non-fat dry milk, after which the membranes were incubated with primary antibodies at 4 °C overnight and subsequently with peroxidase-conjugated secondary antibodies for 1 h. Immunoreactive protein bands were revealed by enhanced chemiluminescence (ECL; Biosharp, BL523B) and densitometrically quantified using ImageJ software.

The panel of primary antibodies used for immunoblotting included anti-CHES1 (Abcam, ab129453; 1:1000), anti-RORA (Immunoway, YT4166; 1:1000), anti-phospho-AKT (Ser473) (Immunoway, YM8304; 1:1000), anti-total AKT (Immunoway, YM8463; 1:1000), anti-PI3K p85 (Selleck, F0294; 1:1000), anti-phospho-PI3K p85/p55 (Tyr467/199) (Immunoway, YP0224; 1:1000), and anti-GAPDH (Immunoway, YM8016; 1:1000) as a loading control.

Chromatin Immunoprecipitation (ChIP) Assay

ChIP assay were conducted using SimpleChIP® Enzymatic Chromatin IP Kit (#9003, CST) following the manufacturing instruction. The primers for the ChIP were listed as following: For region #1: 5'-TGTTACTCTCAGGACACTCACTATG-3', 5'-AAAGATTTATTTTGGCAGTAAGGGA-3'; For region #2: 5'-ATGGAACGGGAAGTCAACTCAGT-3', 5'-TAAGATTCCTGATATCGAGGTAGCT-3'; For region# 3: 5'-

TGTGGAGCTGGGGGGGAATAGTCGA-3', 5'-CGTGCTCATGCAGGGGCGGGA-3'.

Luciferase Reporter Assay

It was performed as described [28]. The activities of firefly luciferase were measured with a luciferase detection kit (Beyotime, RG027). The RORA promoter sequence were cloned with specific primers based on total genome isolated from MDA-MB-231. The primers used for vector construction were listed: 5'-GGGGTACCCCTCAACAGACTGTGGCACCTAAAA-3', 5'-CCCTCGAGCCTTTAAATATGGTCTTTTTTGGGC-3'.

Colony Formation Assay

The clonogenic capacity of cells was evaluated by seeding 1×10^3 cells per well in 6-well plates, followed by a 14-day culture period during which the medium was exchanged at 3-day intervals. When required, the culture medium was additionally supplemented with T0901317 (20 μM) or LY294002 (20 μM). At the end of the culture period, colonies were fixed with 4% paraformaldehyde and stained with 0.1% crystal violet solution. The percentage of colony formation was determined relative to the corresponding untreated controls after normalization.

Cell Viability Assay

Cell viability was monitored using the CCK-8 assay (Biomake, B34302). Cells (2,000/well) in 96-well plates were incubated with 10 μL CCK-8 reagent for 1 h at 37 °C at daily intervals (days 0-5), and absorbance at 450 nm was measured with a Bio-Tek reader.

Transwell Assays

Cell migration and invasion were evaluated using Transwell chambers (Corning, 353097) with 8-μm pore membranes set into 24-well plates. For invasion assessment, the inserts were precoated with Matrigel prior to cell loading, whereas migration assays were performed without matrix coating. Cells were harvested, resuspended in serum-free medium, and added to the upper chambers at a density of 5×10^4 cells per 200 μL. The lower compartments were filled with 600 μL of medium supplemented with 10% FBS to induce chemotaxis. Following 24 h of incubation at 37 °C, the inserts were retrieved, and cells on the inner side of the membrane were gently removed. The cells that had traversed to the outer membrane surface were then fixed with 4% paraformaldehyde for 30 min and stained with 0.1% crystal violet for 20 min. Stained cells were counted under a light microscope in three randomly selected fields per insert.

Wound-Healing Assay

Cell motility was assessed by wound-healing assays. Cells were cultured in 6-well plates until reaching 90-95% confluence, after which a linear gap was introduced across the monolayer with a sterile 200-μL pipette tip. Debris was removed by gentle PBS washing, and the cultures were shifted to serum-free medium for 24 h. Microscopic images were taken at the time of wounding and after incubation, and the extent of migration was quantified as the percentage of wound closure relative to the initial gap area.

Nude Mouse Xenograft Model

Four-week-old female BALB/c nude mice were obtained from GemPharmatech

(Nanjing, China) and maintained under specific pathogen-free conditions. For xenograft establishment, 100 μL of a suspension containing 1×10^7 stably transfected cells (either shCTRL- or shCHES1- expressing) mixed with Matrigel at a 1:1 ratio in PBS was implanted subcutaneously in the vicinity of the fourth mammary fat pad. Tumor sizes were assessed every third day using a digital caliper, and the corresponding volumes were derived from the formula ($V = \text{length}\times\text{width}^2/0.52$). Body weight measurements were taken concurrently at each time point. For drug treatment groups, LY29004 (20 mg/kg, once every three days) or T0901317 (10 μM, once every three days) was injected intratumorally, while the vehicle control groups were administered an equivalent amount of the solvent alone. Mice were euthanized when the maximum tumor volume reached 1500 mm^3, and tumors were excised and weighed.

Immunohistochemistry (IHC)

5-μm paraffin sections of tumor tissues were first dewaxed in xylene and rehydrated through a descending ethanol series. Heat‐induced epitope retrieval was then carried out in citrate buffer (pH 6.0) using a microwave oven. To block endogenous peroxidase activity, the sections were treated with 3% hydrogen peroxide, followed by incubation with 5% goat serum to minimize nonspecific antibody binding. The slides were then probed with primary antibodies against RORA (Immunoway, YT4166; 1:100), Ki67 (CST, 12202; 1:300), and phospho-AKT (Ser473) (Immunoway, YM8304; 1:100) overnight at 4 °C. After rinsing, the sections were exposed to HRP-conjugated secondary antibodies, and immune complexes were visualized with 3,3'-diaminobenzidine (DAB; Genentech, GK600510) as the chromogenic substrate. Finally,

the specimens were counterstained with hematoxylin. For quantitative evaluation, the mean optical density of Ki67 and the mean fluorescence intensity of p-AKT were analyzed using ImageJ software.

Statistical Analysis

A minimum of three independent repetitions was required for each experimental condition. Unless explicitly stated, all values are given as means ± SD. Pairwise and multiple comparisons were respectively handled by Student's t-test and one-way ANOVA, whereas repeated measurements of tumor size over time were assessed via two-way ANOVA with repeated measures. Throughout this work, P-values below 0.05 (*) were taken to indicate significance, and $P < 0.01$ (**) as well as $P < 0.001$ (***) were taken as indicators of greater statistical confidence. GraphPad Prism 8.0 served as the primary platform for all analyses.

Results

Circadian clock component RORA was transcriptionally suppressed by CHES1 in TNBC

Comprehensive RNA-seq from our previously published research [13] revealed that CHES1, served as transcription factor, maintained the tumorigenesis and metastasis through modulating genes expression. Considering that well-documented role of CHES1 as a transcriptional suppressor, we tried to identify the key downstream factor that was suppressed by CHES1 and modulated tumor progression of TNBC. Heatmap showed that there were 1,372 and 2,654 up-regulated genes after CHES1 knockdown in the cell models, MDA-MB-231 and BT549, respectively (Figure 1A-1B). Among

285 these upregulated genes, RORA was significantly upregulated after CHES1 knockdown
286 in both TNBC cells (Figure 1C and 1D), and prognostic analysis demonstrated that
287 patients with high expression of RORA possessed longer survival time (Figure 1E),
288 indicating RORA was a favorable factor in breast cancer. Moreover, literature searching
289 indicated that circadian clock disruption increased the susceptibility and aggressive
290 phenotype of breast cancer, and clock core factor RORA was frequency dysregulated
291 and exhibited tumor-suppressing function in breast cancer [15, 16]. Therefore, we
292 hypothesized that CHES1 maintained its oncogenic role through inhibiting RORA
293 transcription in TNBC. To prove this assumption, lentivirus-mediated knockdown of
294 CHES1 was performed. Immuno-blotting analysis and qPCR showed that knockdown
295 of CHES1 significantly increased RORA expression both in mRNA and protein levels
296 (Figures 1F-1H), indicating the inhibitory effect of CHES1 on RORA mainly on
297 transcription level. To elucidate the detailed mechanism by which CHES1 inhibited
298 RORA transcription, we analyzed the proximal promoter sequence of human RORA.
299 Bioinformatic prediction identified three putative CHES1-binding motifs (located in
300 approximately -337, -740, and -822 bp) located upstream of the transcription start site
301 (Figure 2A). ChIP assays were conducted and verified that the region #1 and #2 had
302 obvious abundance of CHES1 (Figure 2B), indicating CHES1 directly bound to *RORA*
303 promoter to transcriptionally repress RORA expression. In addition, RORA promoter
304 were cloned and constructed into pGL4.10 vector, luciferase reporter gene assay was
305 conducted in HEK-293T cells. The *RORA* promoter luciferase activity was repressed
306 by CHES1 overexpression in a dose-dependent fashion (Figure 2C). Totally, these

results demonstrated that CHES1 operated as a transcriptional repressor of RORA in TNBC.

CHES1 had a negative expression correlation with RORA in TNBC

To investigate the clinical relationship between CHES1 and RORA, we performed IHC on 26 TNBC specimens. Tumors exhibiting positive RORA immunoreactivity generally showed low CHES1 expression, whereas those negative for RORA displayed prominent CHES1 staining, revealing an inverse protein‐ level correlation between the two markers in TNBC (Figure 2D). Additionally, CHES1 and RORA expression levels were found to be significantly inversely associated in the analyzed TNBC patient samples (P=0.0068; Figure 2E). Pearson correlation analysis further confirmed an inverse and statistically significant relationship (r=−0.5175, P=0.0068; Figure 2F). We then detected CHES1 and RORA protein expression in TNBC cell lines. Western blotting revealed that BT549 and MDA-MB-231 exhibited greater abundance of CHES1 but had a lower level of RORA, upregulation of RORA was found in MDA-MB-436 cells that had weak endogenous expression of CHES1 (Figure 2G). In conclusion, these finding indicated that CHES1 expression was inversely correlated with RORA in TNBC.

RORA exerted tumor-suppressive activity in TNBC

Based on the vital role of CHES1 on tumorigenesis in TNBC and the regulatory model between CHES1 and RORA, the functional significance and molecular actions of RORA were further investigated. Firstly, we established stably overexpression model in MDA-MB-231 through lentivirus transfection with Flag-RORA. As shown in Figure 3A and Supplementary 1A, western blotting and qPCR confirmed robust ectopic

expression of RORA in MDA-MB-231. Combined CCK-8 and colony formation analyses revealed that RORA overexpression significantly impaired clonogenicity and proliferation capacity (Figure 3B-3D). Transwell assays and quantification analysis revealed that upregulation of RORA markedly inhibited MDA-MB-231 cell migration and invasion (Figure 3E-3F). In contrast, endogenous RORA expression in MDA-MB-231 cells was suppressed via lentiviral delivery of specific shRNA. The efficiency of this knockdown was subsequently verified by western blotting and qPCR.(Figure 3G and Supplementary 1B). CCK-8 assay found that silencing RORA significantly increased MDA-MB-231 cell viability (Figure 3H). Wound-healing and transwell assays revealed that RORA depletion significantly facilitated the migration and invasion of MDA-MB-231 cells (Figure 3I-3L). In conclusion, these functional gain-and-loss studies demonstrated that RORA served as tumor-repressor and suppressed malignant phenotypes of TNBC cells *in vitro*, which reinforces the findings from CHES1 silencing.

RORA inhibition rescued the CHES1-mediated the malignant phenotype of TNBC

Considering the tumor repressor RORA was transcriptionally suppressed by CHES1 in TNBC, we next to evaluate the effect of RORA inhibition on the CHES1-induced tumorigenesis and metastatic phenotype of TNBC. The selective inhibitor of RORA, T0901317 [29], was introduced to impair RORA activity. Western blot found that T0901317 treatment induced a decreased on the expression of RORA in MDA-MB-231 (supplementary Figure 2A). qPCR analysis demonstrated that T0901317 significantly repressed RORA-mediated transactivation of BMAL1, which is well-documented to be

as a RORA downstream factor and plays central role in circadian rhythm (Figure 4A). These data confirmed the effective inhibition of T0901317 on RORA in TNBC. Colony formation found that CHES1 knockdown significantly repressed colony number of MDA-MB-231, RORA inhibition significantly increased the proliferation activity and rescued the repressing effect of CHES1 knockdown in TNBC cells (Figure 4B-C). Consistently, transwell and wound-healing assays additionally revealed that T0901317 treatment abrogated CHES1 knockdown-induced the inhibition on MDA-MB-231 cell migration and invasion *in vitro* (Figure 4D-4E and Supplementary 2B-2C). Moreover, RORA knockdown by shRNA in MDA-MB-231 also showed similar rescued effect in MDA-MB-231 (Figure 4F-4I and Supplementary 2D-2E). In conclusion, these results revealed that CHES1 maintained the aggressive phenotype of TNBC through repressing RORA transcription and impairing RORA-mediated tumor-suppressing function.

CHES1/RORA axis regulated PI3K/AKT signaling pathway

Furthermore, the downstream signaling pathways regulated by CHES1/RORA axis were investigated. The MDA-MB-231 stably expressed with vector or Flag-RORA were collected and analyzed with RNA-seq, and the volcano plot found that total 827 differentially expressed genes (DEGs) were identified with RORA overexpression (Figure 5A-5B). And the data was integrated with the RNA-seq profile based on shCHES1 or shCTRL in MDA-MB-231 to find the mutually regulated by CHES1 and RORA. Venn diagram and heatmap indicated that 26 and 49 DEGs were mutually upregulated and downregulated in two profiles, respectively (Figure 5C). Furthermore, among the pathways enriched by KEGG analysis of the DEGs, the PI3K/AKT signaling

cascade ranked highest (Figure 5D). Heatmaps revealed that and PI3K/AKT associated DEGs were found in MDA-MB-231 cells with OE-RORA and shCHES1 respectively, suggesting that CHES1/RORA axis modulated the activity of PI3K/AKT pathway (supplementary Figure 3A and 3B). Moreover, immunoblotting analysis also revealed that RORA overexpression or CHES1 knockdown obviously decreased the phosphorylation status of PI3K and AKT in TNBC cells, indicating a large pathway inhibition (Figure 5E-5J). In summary, these data demonstrated that CHES1/RORA axis modulated the PI3K/AKT signaling pathway.

CHES1/RORA/PI3K/AKT axis modulated TNBC proliferation and metastasis *in vitro*

Having established that the CHES1/RORA axis negatively regulates the PI3K/AKT signaling pathway, we next investigated its biological significance in TNBC. Specifically, we sought to determine whether this axis functionally modulates TNBC proliferation and metastasis through the PI3K/AKT cascade. To verify this, we treated the cells with LY294002, a specific PI3K/AKT inhibitor. Western blot analysis confirmed that this treatment markedly attenuated PI3K/AKT pathway activation (Figure 6A). And functional experiments found that inhibition of downstream PI3K/AKT counteracted the effect of OE-RORA on the proliferative and migratory capacities of MDA-MB-231 cells *in vitro* (Figure 6B-6G). Consistently, the inhibitory impact of CHES1 silencing on TNBC cell malignancy was also impaired by pre-treated with LY294002. In addition, we used the PI3K activator 740Y-P [42]. 10 μM 740Y-P were introduced to activate PI3K/AKT pathway in TNBC (supplementary Figure 4A and 4B).

Functional assays demonstrated that 740Y-P partially reversed the suppressive effect of CHES1 knockdown on MDA-MB-231 cell migration and invasion (supplementary Figure 4C-4D). Taken together, Together, these results established that the CHES1/RORA axis governs TNBC progression via the PI3K/AKT cascade.

Targeting the CHES1/RORA/PI3K/AKT axis inhibited TNBC tumorigenesis *in vivo*

To corroborate these observations in vivo, we generated xenograft tumors from MDA-MB-231 cells stably expressing shCTRL or shCHES1, and subsequently administered T0901317 and/or LY294002 to suppress RORA and its downstream signaling, respectively (Figure 7A). CHES1 knockdown markedly inhibited tumor growth relative to the shCTRL group, manifesting as reduced tumor volumes throughout the observation period and decreased final tumor weights (Figures 7B-7D), which is consistent with our previous study [12]. Compared with shCTRL group, the group of shCTRL treated with T0901317 possessed bigger tumor volume and heavier weight (Figure 7B-7D), indicating that T0901317-mediated RORA inhibition impaired its tumor-suppressing effect in TNBC. Moreover, shCHES1 + T0901317 group had stronger growth tendency compared to shCHES1 group (Figure 7B-7D), suggesting that the tumor-suppressing effect of shCHES1-induced RORA overexpression was largely impaired by T0901317. Treatment with LY294002, targeting for PI3K/AKT signaling pathway, caused strongest inhibition on tumorigenesis of TNBC *in vivo*, and no significant difference observed between shCTRL+LY294002 and shCHES1+LY294002 (Figure 7B-7D), indicated that PI3K/AKT signaling pathway

served as the CHES1/RORA axis downstream functional pathway to modulate tumorigenesis of TNBC. Pathological analysis revealed that CHES1 knockdown increased RORA expression and downregulated p-AKT levels in the tumor tissues, accompanied with lower levels of Ki67 (Figure 7F-7H). T0901317 targeted RORA inhibition showed strongest intensity of Ki67 and p-AKT in TNBC slices, and LY294002 treatment induced significantly repression on the Ki67 and p-AKT in tumor tissues (Figure 7F-7H). The IHC analysis was consistent with tumor growth tendency *in vivo*, demonstrated that the transcriptional regulatory axis between CHES1 and RORA modulated the tumorigenesis of TNBC through tuning PI3K/AKT signaling pathway. Body weight monitoring showed no obvious systemic toxicity in any treatment group (Figure 7E-7F), indicating that targeting the CHES1/RORA/PI3K/AKT axis might be a strategy for TNBC.

Discussion

The initiation and progression of TNBC is frequently along with aberrant activation of potent oncogenic systems including oncogene activation and inactivation of tumor suppressor genes, apprehensive understanding for this network will be beneficial to target therapy and drug design. CHES1 belongs to Forkhead box (FOX) transcription factor family, ChIP-seq and structurally studies indicated that CHES1 exhibited bilateral regulation on transcription through simultaneously recognizing a canonical forkhead (FKH) motif and a related lower affinity (FHL) motif, contributing it as a bispecific factor in different tissues or cellular context [30]. CHES1-mediated regulation on gene expression and signaling transduction played vital role in organ development,

pulmonary fibrosis, and tumorigenesis[8, 9].Although CHES1 has been established as a critical oncogenic driver in TNBC, primarily through the transcriptional activation of pro-metastatic genes including SNAI1, MMP9, and PDGFD [13], the key downstream effectors that sustain its malignant phenotype remain incompletely defined. Notably, CHES1 is capable of recruiting the SIN3A/histone deacetylase (HDAC) corepressor complex to silence target gene expression [31]. However, its direct tumor-suppressive targets in TNBC have not been systematically identified. This study uncovered that the circadian gene RORA was transcriptionally suppressed by CHES1 and its expression had inverse correlation with CHES1. Functionally, RORA inhibition partially rescued CHES1-mediated aggressive phenotypes of TNBC, indicating that RORA served as the downstream effector of CHES1 in TNBC. As an orphan nuclear receptor, RORA modulates target gene transcription through co-factor interactions, functioning as either an activator or a repressor, it participates in many cancer-associated signaling pathways including metabolic reprogramming, oxidation stress response, and immune infiltration [14]. Increasing evidence demonstrated that RORA could serve as prognostic biomarker and exhibited tumor-suppressing effect and in types of carcinomas, it was frequently downregulated or loss-of-function in cancer tissues [19, 20, 21]. Consistent with these, clinical correlation analyses demonstrated a striking inverse association between CHES1 and RORA protein abundance in human TNBC specimens, indicating that CHES1-mediated RORA repression is a defining feature of this disease. Mechanistically, CHES1 could directly bond on the promoter of *RORA* and transcriptionally inhibited its transcription. In addition, functional experiments

461 confirmed that RORA suppressed proliferation and invasion of TNBC cells, extending
462 its previously reported tumor-suppressive functions in breast cancer [17, 18] to the triple-
463 negative subtype. These findings extend the current understanding of CHES1
464 oncogenic function. Beyond acting as an activator of proliferative signaling, CHES1
465 actively orchestrates tumorigenesis by extinguishing a pivotal tumor-suppressive
466 circadian program. Natural compound Nobiletin could inhibit IκB/NFκB signaling
467 through activating RORs-mediated anti-tumor effect in TNBC, but Nobiletin was not a
468 selective activator for RORA [25]. Therefore, developing novel specific CHES1 inhibitor
469 or RORA agonist might be a promising strategy.
470 Moreover, this study also revealed the CHES1/RORA-regulated signaling pathway in
471 TNBC through conjoint analysis of transcriptome profiles. We identified that
472 PI3K/AKT, a firm and classical oncogenic signaling pathway in various tumors, was
473 orchestrated by CHES1 and RORA in TNBC. Our results found that CHES1
474 knockdown or RORA overexpression significantly repressed PI3K/AKT activation in
475 TNBC cells, and pharmaceutical inhibition or activation on PI3K/AKT could rescue the
476 aggressive phenotypes of TNBC, indicating that PI3K/AKT was downstream functional
477 pathway of CHES1/RORA. As a conventional phosphorylation-dependent cascade
478 signaling, the activity of PI3K/AKT is largely dependent on the complex signaling
479 transduction and crosstalk during the tumorigenesis and progression of cancers [32].
480 Transcription factors, for example, FOXOs, NFκB, STAT3, and p53, modulated
481 PI3K/AKT activation by regulating transcription of PTEN, p110β, AKT or crosstalking
482 with other signal pathways [32, 33, 34, 35], and PI3K/AKT could facilitate phosphorylation

of FOXOs and p53, formed a feedback loop in tumorigenesis. Considering that CHES1 and RORA have been reported to be phosphorylated and the phosphorylation further affect their activity, whether these regulation model exists between PI3K/AKT and CHES1/RORA in TNBC is needed for further investigation.

Circadian clock disruption is closely associated with tumorigenesis and therapeutic resistance of breast cancer [15, 16]. RORA, accompanied with REV-ERB competitively transactivates BMAL1 expression to control the rate of circadian rhythm. RORA can response to circadian rhythm and modulate energetic metabolism [14, 20]. Moreover, metabolism-associated genes are tended to control or response to circadian rhythm. Our data found that CHES1 directly suppressed RORA expression and knockdown of CHES1 increased BMAL1 transcription in MDA-MB-231 (Figure 4A), indicating CHES1 might be involved in the regulation of circadian rhythm in TNBC. Moreover, previous studies demonstrated that glucose metabolism in liver was regulated by FOXN3 in zebrafish models [36], and the rs8004664 variation within the CHES1 may modulate insulin sensitivity and hyperglycemic risk in women [37]. Therefore, the hypothesis that CHES1 might modulate the glucose utilization and circadian rhythm in TNBC, making it as a multiple functional effector in tumorigenesis. Detailed mechanism and what a role of RORA in this network remains comprehensive evaluation.

In addition, RORA dysfunction mediated circadian clock disruption or transcriptional disorder induced anti-tumor immunotherapy deficiency by increasing PD-L1 expression or decreasing the activity of immune effective cells [38], and our RNA-seq data also revealed that RORA-associated DEGs were enriched in immunity related

pathways, such as cytokine-cytokine receptor interaction, IL-17 signaling and natural killer cell mediated cytotoxic (supplementary Figure 3C), so the defined role of CHES1/RORA axis in immunotherapy of TNBC is also promising research in the future. In summary, this work identified the core circadian factor RORA as a critical downstream effector of CHES1 in TNBC. We demonstrated that the CHES1/RORA axis promoted TNBC progression by activating the PI3K/AKT signaling pathway (Figure 8)[39]. These findings expanded the current understanding of CHES1 and RORA functions and provided a mechanistic insight into TNBC heterogeneity. While further validation is required, targeting the CHES1/RORA-mediated PI3K/AKT signaling cascade offers a putative molecular basis and a translational entry point for the development of targeted therapies against TNBC.

Acknowledgements

This work was financially supported by Taishan Scholars Program of Shandong Province (tsqn2021031129), the Natural Science Foundation of Shandong Province (ZR2024QKC251, ZR2024QH657), the special Funding for the “Case-by-Case-Introduction of Top Talent (Teams)” Program in Yantai. The Leading Talents above Provincial Level in Yantai, Health Technology Innovation Team Construction Project of Shandong Province, Fundamental Research Projects of Science & Technology Innovation and Development Plan in Yantai City (2024JCYJ096), Shandong Province Medical and Health Technology Development Plan Project (202404070013), 2024 Annual Special Scientific Innovation Project on Traditional Chinese Medicine of Binzhou Medical University (2024ZYYZX04), and grants (BY2022KYQD12) from

Shandong Medical and pharmaceutical university. Guizhou Provincial Science and Technology Projects (QKHJC-2024-Youth 268), Doctor Start-up Fund of Affiliated Hospital of Guizhou Medical University (gyfybsky-2024-39).

Competing interests

The authors confirm that they have no conflicts of interest.

Data availability statement

The raw RNA-seq transcriptome sequencing data generated in this study have been deposited in GSA-Human (Genome Sequence Archive for human data) of the National Genomics Data Center (NGDC), China National Center for Bioinformation / Beijing Institute of Genomics, Chinese Academy of Sciences, and are publicly accessible at (https://ngdc.cncb.ac.cn/gsa-human/). This study has been assigned the accession number HRA019400[40, 41]. The original data and materials supporting the findings of this study are accessible upon reasonable request to the corresponding author.

Ethics approval statement

All the slices for IHC collected from Yantai Affiliated Hospital of Shandong Medical and Pharmaceutical University, all individuals who donated tissues for this study provided written informed consent, which was approved the Ethics Committee for Biology and Medical Science of Shandong Medical and Pharmaceutical University (Approval No. 2024-131). Animal studies were performed in accordance with institutional guidelines and with the approval of the Institutional Animal Care and Use Committee (Approval No. 2024-243).

Author contribution Statement

P.F.W., Y.Y.Y., and Z.W.X. conceived the study. Y.J.W., Z.W.X., D.M.K., and Y.M. designed the methodology. Y.J.W., Z.W.X., D.M.K., and Y.X.X. performed experiments and validation. Y.J.W., Z.W.X., D.M.K., and X.J.T. conducted formal analysis and software. P.F.W., G.L.Z., and Y.Y.Y. provided resources and funding. Y.J.W., Z.W.X., and Y.Y.Y. wrote the original draft; P.F.W., Z.W.X., and Y.Y.Y. reviewed and edited the manuscript. Y.J.W., Z.W.X. prepared figures. P.F.W., G.L.Z., and Y.Y.Y. supervised the study and administered the project. All authors approved the final version.

References

1. Liedtke C, Mazouni C, Hess KR, André F, Tordai A, Mejia JA*, et al.* Response to Neoadjuvant Therapy and Long-Term Survival in Patients With Triple-Negative Breast Cancer. *Journal of Clinical Oncology* 2008, **26**(8)**:** 1275-1281.

2. Choupani E, Mahmoudi Gomari M, Zanganeh S, Nasseri S, Haji-allahverdipoor K, Rostami N*, et al.* Newly Developed Targeted Therapies Against the Androgen Receptor in Triple-Negative Breast Cancer: A Review. *Pharmacological Reviews* 2023, **75**(2)**:** 309-327.

3. Li Y, Zhang H, Merkher Y, Chen L, Liu N, Leonov S*, et al.* Recent advances in therapeutic strategies for triple-negative breast cancer. *Journal of Hematology & Oncology* 2022, **15**(1)**:** 121.

4. Verma S, Singh V, Lang JE, Gupta S. Reprogramming the immune microenvironment in triple-negative breast cancer with mRNA therapeutics. *Cancer Letters* 2026, **645:** 218350.

5. So JY, Ohm J, Lipkowitz S, Yang L. Triple negative breast cancer (TNBC): Non-genetic tumor heterogeneity and immune microenvironment: Emerging treatment options. *Pharmacology & Therapeutics* 2022, **237:** 108253.

6. Zema S, Di Fazio F, Pelullo M, Di Savino S, Cerbelli B, Leopizzi M*, et al.* MAML1 drives Notch and Hedgehog oncogenic pathways by inhibiting Itch activity in triple-negative breast cancer. *Cell Death & Differentiation* 2025, **33**(5)**:** 971-987.

7. Du J, Jin L, Wang S, Hu X, Yu J, Yu J*, et al.* FOXN3 integrates the KU70/KU80/SREBP-1 complex to regulate lipid metabolism in non-alcoholic fatty liver disease. *Nucleic Acids Research* 2026, **54**(5)**:** gkag171.

8. Yu J, Li Y, Li Y, Liu X, Huo Q, Wu N*, et al.* Phosphorylation of FOXN3 by NEK6 promotes pulmonary fibrosis through Smad signaling. *Nature Communications* 2025, **16**(1)**:** 1865.

9. Zhu X, Huo Q, Jin L, et al. PARP1 stabilizes FOXN3 to suppress pulmonary fibrosis through p38-related feedback regulation. Sci Adv. 2026;**12**(1)**:** eady1681.

10. Zhu X, Huang B, Zhao F, Lian J, He L, Zhang Y*, et al.* p38-mediated FOXN3 phosphorylation modulates lung inflammation and injury through the NF-κB signaling pathway. *Nucleic Acids Research* 2023, **51**(5)**:** 2195-2214.

11. Liu X, Zeng Q, Yang H, Li W, Chen Q, Yin K*, et al.* Single-Nucleus Multiomic Analyses Identifies Gene Regulatory Dynamics of Phenotypic Modulation in Human Aneurysmal Aortic Root. *Advanced Science* 2024, **11**(22)**:** e2400444.

12. Xu Z, Yang Y, Li B, Li Y, Xia K, Yang Y*, et al.* Checkpoint suppressor 1 suppresses

transcriptional activity of ERα and breast cancer cell proliferation via deacetylase SIRT1. *Cell Death & Disease* 2018, **9**(5)**:** 559.

13. Xu Z, Liu S, Feng C, Xu F, Kong D, Mi J*, et al.* Acetylation of Checkpoint suppressor 1 enhances its stability and promotes the progression of triple-negative breast cancer. *Cell Death Discovery* 2022, **8**(1)**:** 474.

14. Lee JM, Kim H, Baek SH. Unraveling the physiological roles of retinoic acid receptor-related orphan receptor α. *Experimental & Molecular Medicine* 2021, **53**(9)**:** 1278-1286.

15. Zhang Y, Zhang Q, Liu R, Zhang D, Hu G, Chen X. Circadian disruption in cancer and regulation of cancer stem cells by circadian clock genes: An updated review. *Cancer Letters* 2025, **611:** 217391.

16. He LH, Sui XY, Xiao YL, Ji P, Gong Y. Circadian Rhythm Disruption in Triple-Negative Breast Cancer: Molecular Insights and Treatment Strategies. *Journal of Pineal Research* 2025, **77**(3): e70042.

17. Xiong G, Xu R. Retinoid orphan nuclear receptor alpha (RORα) suppresses the epithelial–mesenchymal transition (EMT) by directly repressing Snail transcription. *Journal of Biological Chemistry* 2022, **298**(7): 102059.

18. Xiong G, Wang C, Evers BM, Zhou BP, Xu R. RORα Suppresses Breast Tumor Invasion by Inducing SEMA3F Expression. *Cancer Research* 2012, **72**(7)**:** 1728-1739.

19. Liu H, Li Y, Tang L, Sun X, Xie W, Xiao T*, et al.* UBR5 metabolically reprograms

610 nasopharyngeal carcinoma cells to promote glycolysis and M2 polarization via
611 SPLUNC1 signaling. *npj Precision Oncology* 2024, **8**(1): 252.

612 20. Yao W, Shang L, Wang Y, Xu L, Bai Y, Feng M*, et al.* DNMT1-driven methylation of RORA
613 facilitates esophageal squamous cell carcinoma progression under hypoxia through
614 SLC2A3. *Journal of Translational Medicine* 2024, **22**(1): 1167.

615 21. Yang J, Lin J, Guo H, Wu W, Wang J, Mao J*, et al.* Administration of statins is correlated
616 with favourable prognosis in lung cancer patients receiving immune checkpoint
617 inhibitors. *Frontiers in Immunology* 2025, **16:** 1638677.

618 22. Liu D, Wei B, Liang L, et al. The Circadian Clock Component RORA Increases
619 Immunosurveillance in Melanoma by Inhibiting PD-L1 Expression. Cancer Res. 2024,
620 **84**(14): 2265-2281.

621 23. Mao W, Xiong G, Wu Y, Wang C, St. Clair D, Li J-D*, et al.* RORα Suppresses Cancer-
622 Associated Inflammation by Repressing Respiratory Complex I-Dependent ROS
623 Generation. *International Journal of Molecular Sciences* 2021, **22**(19): 10665.

624 24. Taheri M, Omrani MD, Noroozi R, Ghafouri-Fard S, Sayad A. Retinoic acid-related
625 orphan receptor alpha (RORA) variants and risk of breast cancer. *Breast Disease* 2017,
626 **37**(1)**:** 21-25.

627 25. Kim E, Kim Y-J, Ji Z, Kang JM, Wirianto M, Paudel KR*, et al.* ROR activation by Nobiletin
628 enhances antitumor efficacy via suppression of IκB/NF-κB signaling in triple-negative
629 breast cancer. *Cell Death & Disease* 2022, **13**(4): 374.

630 26. Bullock KK, Shattuck-Brandt R, Scalise C, Luo W, Chen S-C, Saleh N*, et al.* Endogenous
631 pAKT activity is associated with response to AKT inhibition alone and in combination
632 with immune checkpoint inhibition in murine models of TNBC. *Cancer Letters* 2024,
633 **586:** 216681.

634 27. Tu Z, Hu Y, Raizada D, Bassal MA, Tenen DG, Karnoub AE. Long noncoding RNA–
635 mediated activation of PROTOR1/PRR5-AKT signaling shunt downstream of PI3K
636 in triple-negative breast cancer. *Proceedings of the National Academy of Sciences* 2022,
637 **119**(43)**:** e2203180119.

638 28. Feng C, Kong D, Tong B, Liang Y, Xu F, Yang Y*, et al.* Hypoxia-triggered ERRα acetylation
639 enhanced its oncogenic role and promoted progression of renal cell carcinoma by
640 coordinating autophagosome-lysosome fusion. *Cell Death & Disease* 2025, **16**(1)**:** 23.

641 29. Kumar N, Solt LA, Conkright JJ, Wang Y, Istrate MA, Busby SA*, et al.* The
642 Benzenesulfoamide T0901317 [N-(2,2,2-Trifluoroethyl)-N-[4-[2,2,2-trifluoro-1-
643 hydroxy-1-(trifluoromethyl)ethyl]phenyl]-benzenesulfonamide] Is a Novel Retinoic
644 Acid Receptor-Related Orphan Receptor-α/γ Inverse Agonist. *Molecular*
645 *Pharmacology* 2010, **77**(2)**:** 228-236.

646 30. Xu Y, Liu J, Tian Y, Wang Z, Song Z, Li K*, et al.* Wnt/β-Catenin Signaling Pathway Is
647 Strongly Implicated in Cadmium-Induced Developmental Neurotoxicity and
648 Neuroinflammation: Clues from Zebrafish Neurobehavior and In Vivo Neuroimaging.
649 *International Journal of Molecular Sciences* 2022, **23**(19)**:** 11434.

650 31. Li W, Zhang Z, Liu X, Cheng X, Zhang Y, Han X*, et al.* The FOXN3-NEAT1-SIN3A repressor

complex promotes progression of hormonally responsive breast cancer. *Journal of Clinical Investigation* 2017, **127**(9)**:** 3421-3440.

32. He Y, Sun MM, Zhang GG, Yang J, Chen KS, Xu WW*, et al.* Targeting PI3K/Akt signal transduction for cancer therapy. *Signal Transduction and Targeted Therapy* 2021, **6**(1)**:** 425.

33. Rani M, Kumari R, Singh SP, Devi A, Bansal P, Siddiqi A*, et al.* MicroRNAs as master regulators of FOXO transcription factors in cancer management. *Life Sciences* 2023, **321:** 121535.

34. Tsuji T, Maeda Y, Kita K, Murakami K, Saya H, Takemura H*, et al.* FOXO3 is a latent tumor suppressor for FOXO3-positive and cytoplasmic-type gastric cancer cells. *Oncogene* 2021, **40**(17)**:** 3072-3086.

35. Wiese W, Barczuk J, Racinska O, Siwecka N, Rozpedek-Kaminska W, Slupianek A*, et al.* PI3K/Akt/mTOR Signaling Pathway in Blood Malignancies—New Therapeutic Possibilities. *Cancers* 2023, **15**(21)**:** 5297.

36. Karanth S, Adams JD, Serrano MdlA, Quittner-Strom EB, Simcox J, Villanueva CJ*, et al.* A Hepatocyte FOXN3-α Cell Glucagon Axis Regulates Fasting Glucose. *Cell Reports* 2018, **24**(2)**:** 312-319.

37. Erickson ML, Karanth S, Ravussin E, Schlegel A. FOXN3 hyperglycemic risk allele and insulin sensitivity in humans. *BMJ Open Diabetes Research & Care* 2019, **7**(1).

38. Akashi M, Takumi T. The orphan nuclear receptor RORα regulates circadian

transcription of the mammalian core-clock Bmal1. *Nature Structural & Molecular Biology* 2005, **12**(5)**:** 441-448.

39. Jiang S, Li H, Zhang L, Mu W, Zhang Y, Chen T*, et al.* Generic Diagramming Platform (GDP): a comprehensive database of high-quality biomedical graphics. *Nucleic Acids Research* 2025, **53**(D1)**:** D1670-D1676.

40. Zhang S, Chen X, Jin E, et al. The GSA Family in 2025: A Broadened Sharing Platform for Multi-omics and Multimodal Data. Genomics Proteomics Bioinformatics. 2025;**23**(4)**:** qzaf072.

41. Bao Y, Zhang Z, Zhao W, Xiao J, Song S, He S*, et al.* Database resources of the National Genomics Data Center, China National Center for Bioinformation in 2026. *Nucleic Acids Research* 2026, **54**(D1)**:** D28-D47.

42. Ren R, Zhang S, Peng Z, et al. Matrix stiffness regulates glucose-6-phosphate dehydrogenase expression to mediate sorafenib resistance in hepatocellular carcinoma through the ITGB1-PI3K/AKT pathway. Cell Death Dis. 2025;**16**(1):538.

692 **Figure legends**

693 **Figure 1. RNA-seq analysis and experimental validation indicated that RORA was**
694 **the downstairs factor of CHES1 in TNBC. (A-B)** Heatmaps showing global
695 differentially expressed genes (DEGs) upon CHES1 knockdown (sh-CHES1) versus
696 control (sh-CTRL) in MDA-MB-231 **(A)** and BT549 **(B)** TNBC cell lines. Red
697 indicates upregulated genes, blue indicates downregulated genes. **(C-D)** Volcano plots
698 illustrating transcriptomic changes after CHES1 silencing in MDA-MB-231 **(C)** and
699 BT549 (D) The x-axis represents log2(Fold change), and the y-axis represents
700 −log10(P-value). RORA is marked as a significantly upregulated gene in both cell lines.
701 Red dots: significantly upregulated DEGs; blue dots: significantly downregulated
702 DEGs; gray dots: non-differentially expressed genes. **(E)** Kaplan–Meier survival curve
703 of patients with breast invasive carcinoma stratified by RORA expression levels.
704 Patients with low RORA expression exhibit significantly shorter survival times
705 compared to those with high RORA expression (n=26 for high RORA group, n=24 for
706 low RORA group; $P<0.0001$). **(F)** qRT-PCR quantification of relative RORA mRNA
707 levels in sh-CTRL and sh-CHES1 BT549 and MDA-MB-231 cells. RORA mRNA is
708 markedly elevated upon CHES1 depletion. Data are presented as mean ± SD; ***P <
709 0.001.**(G-H)** Western blot analysis of CHES1 and RORA protein expression in BT549
710 **(G)** and MDA-MB-231 **(H)** cells with or without CHES1 knockdown. GAPDH serves
711 as the internal loading control. Silencing CHES1 robustly increases RORA protein
712 abundance in both TNBC cell lines.

713 **Figure 2. CHES1 directly suppressed the RORA transcription and had negative**

expression correlation with RORA in TNBC. (A) Predicted conserved CHES1 binding motif and schematic diagram of three candidate binding regions (#1, #2, #3) within the 1 kb upstream sequence of the RORA promoter. Red triangles indicate CHES1 binding sites. **(B)** ChIP-qPCR assay verifying the direct binding of CHES1 on the three predicted regions on the RORA promoter in MDA-MB-231 cells. IgG is used as the negative control. Relative fold enrichment of CHES1-bound DNA fragments is quantified. *$P < 0.05$, **$P < 0.01$, ***$P < 0.001$. **(C)** Luciferase reporter assay using the RORA-promoter luc and PGL4.10 luc construct showed the effect of CHES1 on the RORA transcription. **$P < 0.01$, ***$P < 0.001$. **(D)** Representative immunohistochemical (IHC) staining images of CHES1 and RORA in human TNBC tissue specimens. Scale bar = 50 μm. **(E)** Pearson correlation scatter plot showing the negative linear correlation between CHES1 and RORA expression levels in TNBC clinical tissues (r = -0.5175, P=0.0068). **(F)** Contingency table presenting the association between CHES1 and RORA protein expression status in 26 TNBC patient samples, analyzed by Chi-square test (P=0.0068). **(G)** Western blot showed the endogenous CHES1 and RORA protein abundance in four TNBC cell lines (SUM159, MDA-MB-436, MDA-MB-231, BT549). GAPDH was used as internal reference. The numerical values below each band represent the relative gray intensity normalized to SUM159 cells.

Figure 3. RORA inhibited the proliferation and metastasis of TNBC in vitro. (A) Western blot validated the efficiency of RORA overexpression (OE-RORA) in MDA-MB-231 cells, with OE-CTRL as empty vector control; GAPDH served as loading

control. **(B)** CCK-8 cell viability assay showed that overexpression of RORA significantly suppressed the proliferative capacity of MDA-MB-231 cells over 6 days. ***$P < 0.001$. **(C-D)** Representative images **(C)** and quantitative statistics **(D)** of colony formation assay. Ectopic RORA expression markedly reduced the colony number of MDA-MB-231 cells. **$P < 0.01$. **(E-F)** Transwell assay **(E)** and corresponding quantitative analysis **(F)**showed the effect of RORA overexpression on the migration and invasion of MDA-MB-231 cells. (scale bar = 100 μm). Overexpressing RORA impaired the migratory and invasive abilities **$P < 0.01$. **(G)** Western blot confirmed the knockdown efficiency of sh-RORA in MDA-MB-231 cells, with sh-CTRL as negative control; GAPDH was used as internal reference. **(H)** CCK-8 proliferation curve demonstrated that RORA silencing notably promoted cell viability of MDA-MB-231 cells. *$P < 0.05$. **(I-J)** Wound-healing **(I)** and quantitative migration area statistics **(J)** found that loss of RORA accelerated the migration of MDA-MB-231 cells. **$P < 0.01$. **(K-L)** Transwell assay **(K)** and quantitative quantification **(L)** showed that knockdown of RORA significantly enhanced the migration and invasion phenotypes of TNBC cells. **$P < 0.01$.

Figure 4. Inhibition or knockdown of RORA rescued the effect of shCHES1 on the proliferation and metastasis in TNBC. (A) q-PCR detected the relative BMAL1 mRNA expression in four indicated groups of MDA-MB-231 cells treated with or without T0901317. *$P < 0.05$, **$P < 0.01$.**(B-C)** Representative colony formation images **(B)** and quantitative statistics of relative colony numbers **(C)**. ns, not significant; *$P < 0.05$, **$P < 0.01$. **(D-E)** Crystal violet staining images of Transwell migration and

758 invasion assays (scale bar = 100 μm) **(D)** and quantitative analysis showed the relative
759 migratory and invasive cell ratios **(E)**. ns, not significant; *$P < 0.05$, **$P < 0.01$. And
760 Supplementary Figure2B-2C **(F-G)** Representative colony formation images **(F)** and
761 quantitative statistics of colony number **(G)** showed the effect of RORA knockdown on
762 the colony formation activity of MDA-MB-231 cells . ns, not significant; *$P < 0.05$,
763 **$P < 0.01$. **(H-I)** Transwell **(H)** and quantitative statistics **(I)** showed the relative
764 migration and invasion rates of four indicated groups (scale bar = 100 μm). ns, not
765 significant; *$P < 0.05$, **$P < 0.01$.

766 **Figure 5. Integrated analysis of RNA-seq indicated that CHES1/RORA axis**
767 **regulated the activity of PI3K/AKT signaling pathway in TNBC. (A)** Schematic
768 workflow of RNA-seq and subsequent bioinformatics analysis. **(B)** Volcano plot
769 showed the differentially expressed genes (DEGs) between OE-RORA and OE-CTRL
770 groups. Red dots represent significantly upregulated genes (379), blue dots represent
771 significantly downregulated genes (448), black dots denote genes with no significant
772 expression change. **(C)** Venn diagram displaying the overlapping and unique DEGs
773 among two transcriptome profiles. **(D)** Bubble plot showed that common DEGs from
774 two transcriptome profiles were enriched in pathways based on KEGG enrichment
775 analysis. **(E)** Western blot detection of RORA, phosphorylated PI3K (P-PI3K), total
776 PI3K, phosphorylated AKT (P-AKT) and total AKT protein levels in OE-CTRL and
777 OE-RORA MDA-MB-231 cells. GAPDH served as the internal loading control. **(F)**
778 Western blot analysis of CHES1, P-PI3K, total PI3K, P-AKT and total AKT protein
779 expression in sh-CTRL and sh-CHES1 MDA-MB-231 cells. GAPDH was used as

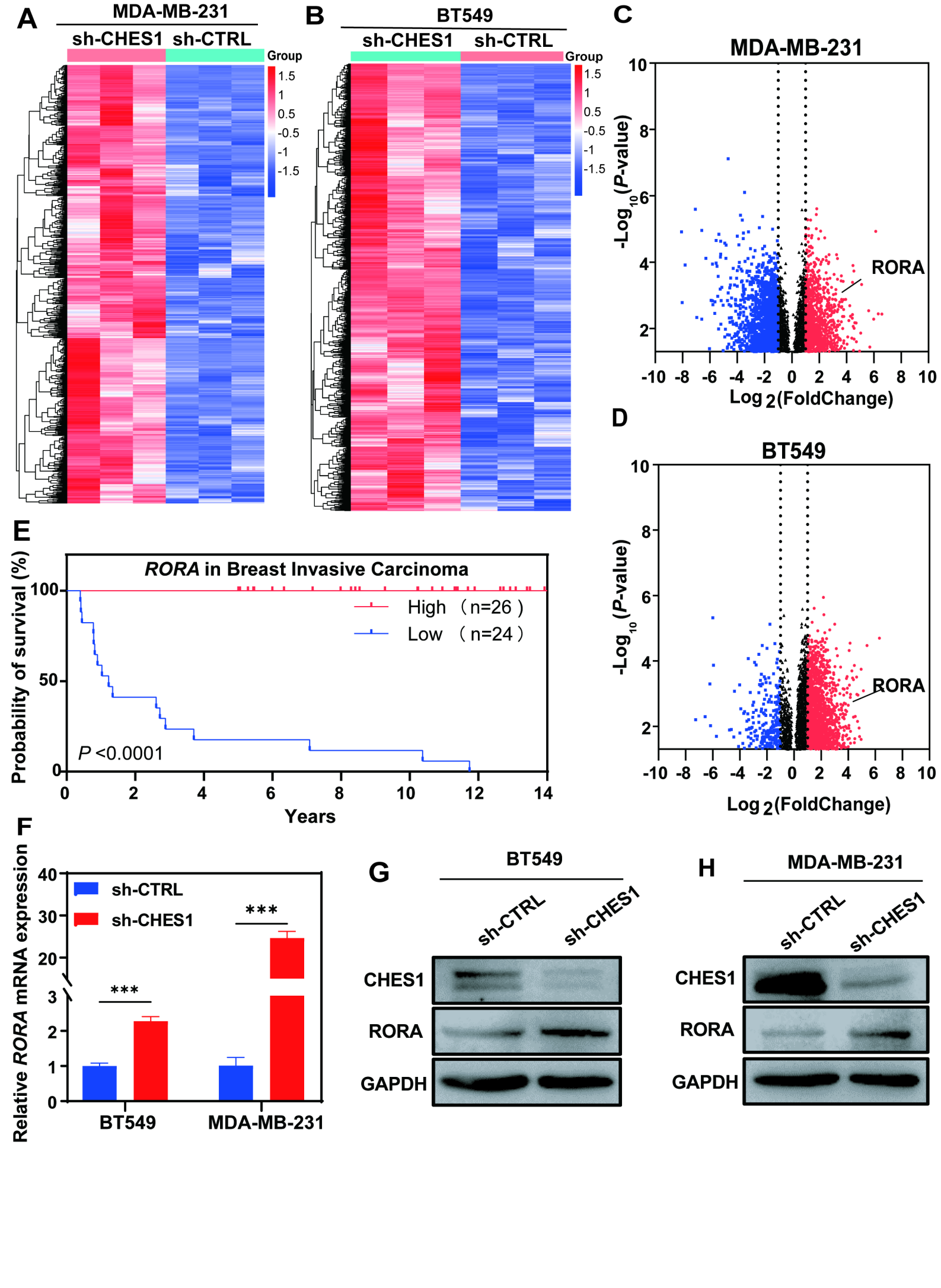
internal reference protein. **(G)** Quantitative statistical analysis of relative p-AKT protein abundance in OE-CTRL and OE-RORA groups. $^{**}P < 0.01$. **(H)** Quantitative statistics of relative P-PI3K protein level in OE-CTRL and OE-RORA groups. $^{*}P < 0.05$. **(I)** Quantitative analysis of relative P-AKT protein expression in sh-CTRL and sh-CHES1 groups. $^{*}P < 0.05$. **(J)** Quantitative statistics of relative P-PI3K protein abundance in sh-CTRL and sh-CHES1 groups. $^{***}P < 0.001$.

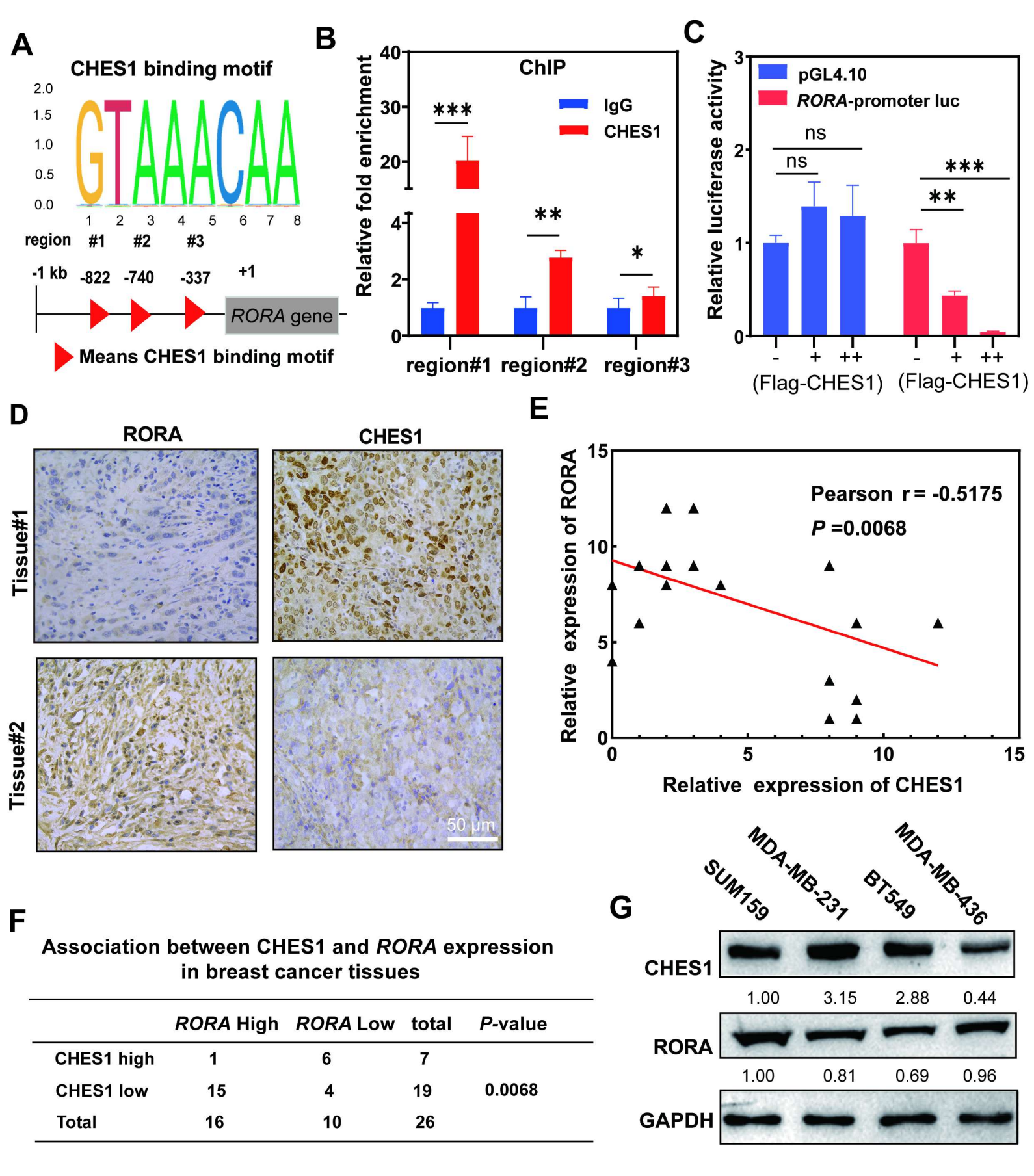
Figure 6. PI3K/AKT was the downstream effective pathway of CHES1/RORA axis in TNBC. (A) Western blot analysis of phosphorylated PI3K (P-PI3K), total PI3K, phosphorylated AKT (P-AKT) and total AKT protein expression in four indicated groups of MDA-MB-231 cells. **(B-C)** Representative bright-field images of colony formation assay **(B)** and quantitative statistics of relative colony numbers **(C)**. ns, not significant; $^{*}P < 0.05$, $^{**}P < 0.01$. **(D-E)** Wound-healing micrographs captured at 0 h and 24 h (D) and quantitative analysis of relative migration area percentage **(E)**. ns, not significant; $^{*}P < 0.05$, $^{***}P < 0.001$. **(F-G)** Crystal violet staining images of Transwell migration and invasion assays (scale bar = 100 μm) **(F)** and quantitative statistics of relative migratory and invasive cell ratios **(G)**. ns, not significant; $^{*}P < 0.05$, $^{**}P < 0.01$.

Figure 7. CHES1/RORA axis-mediated PI3K/AKT activity regulated the tumorigenesis of TNBC *in vivo*. (A) Schematic diagram of the *in vivo* subcutaneous xenograft tumor model establishment using MDA-MB-231 cells and drug administration schedule. Tumor inoculation, intraperitoneal injection of T0901317 (10 mg/kg) or LY294002 (10 μm) were performed at indicated time points, followed by

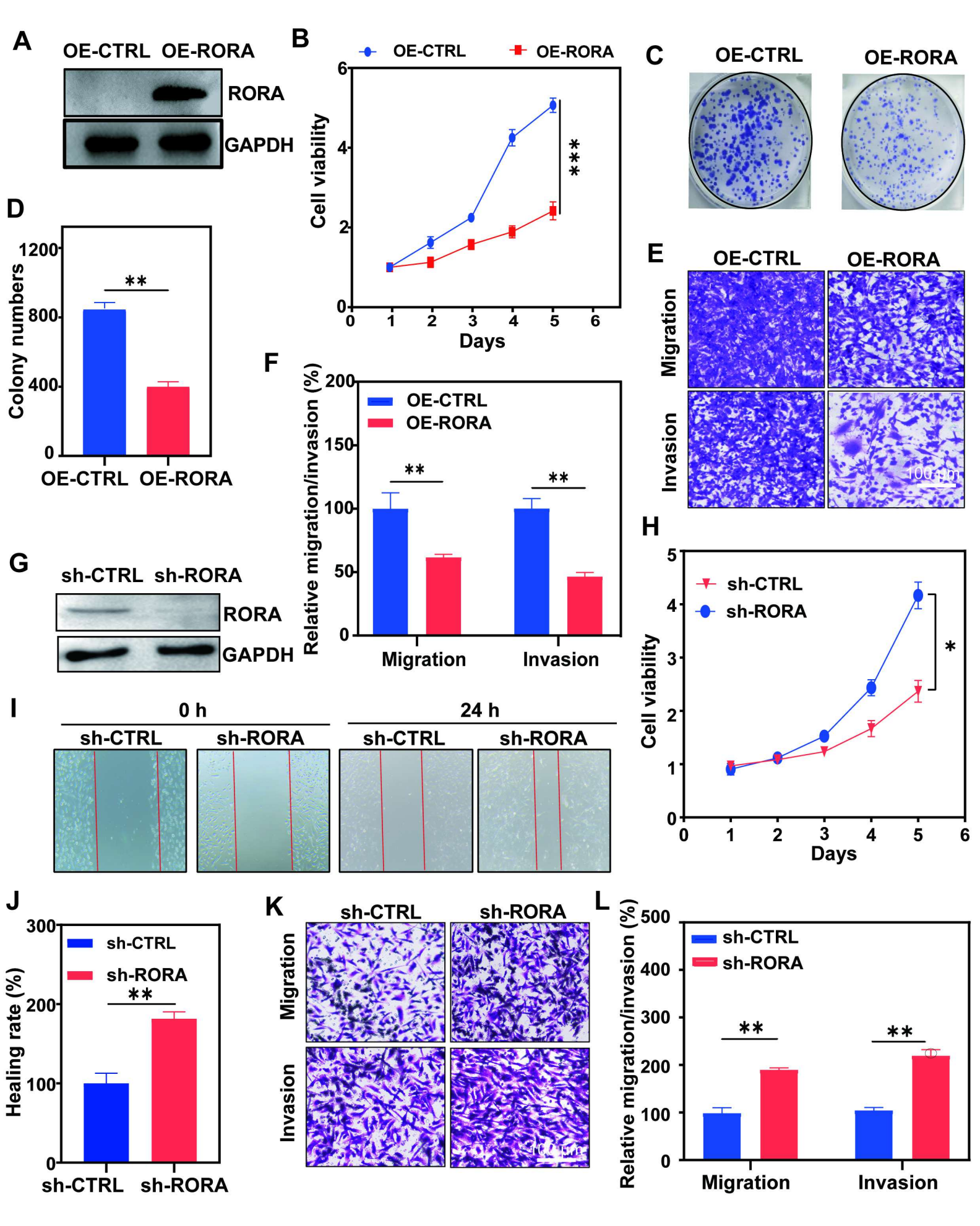
sample collection and analysis on 28th day post injection. **(B)** Images of xenograft tumors excised from six experimental groups at the endpoint of the animal study. **(C)** Dynamic growth curves of tumor volume measured every 4 days over 28 days for each group. $^{**}P < 0.01$, $^{***}P < 0.001$. **(D)** Quantitative statistical analysis of the final tumor weight isolated from six groups. $^{*}P < 0.05$, $^{**}P < 0.01$, $^{***}P < 0.001$. **(E)** Body weight monitoring curve of nude mice during the whole experimental period to evaluate drug biosafety. **(F)** Representative immunohistochemical staining images of RORA and Ki-67, and immunofluorescence staining of P-AKT in xenograft tumor tissues from six groups. **(G)** Quantitative analysis of mean optical density (MOD) of Ki-67 immunohistochemical staining to reflect tumor proliferative activity. $^{*}P < 0.05$, $^{**}P < 0.01$, $^{***}P < 0.001$. **(H)** Quantification of mean fluorescence intensity (MFI) of p-AKT immunofluorescence in tumor tissues. $^{*}P < 0.05$, $^{**}P < 0.01$, $^{***}P < 0.001$.

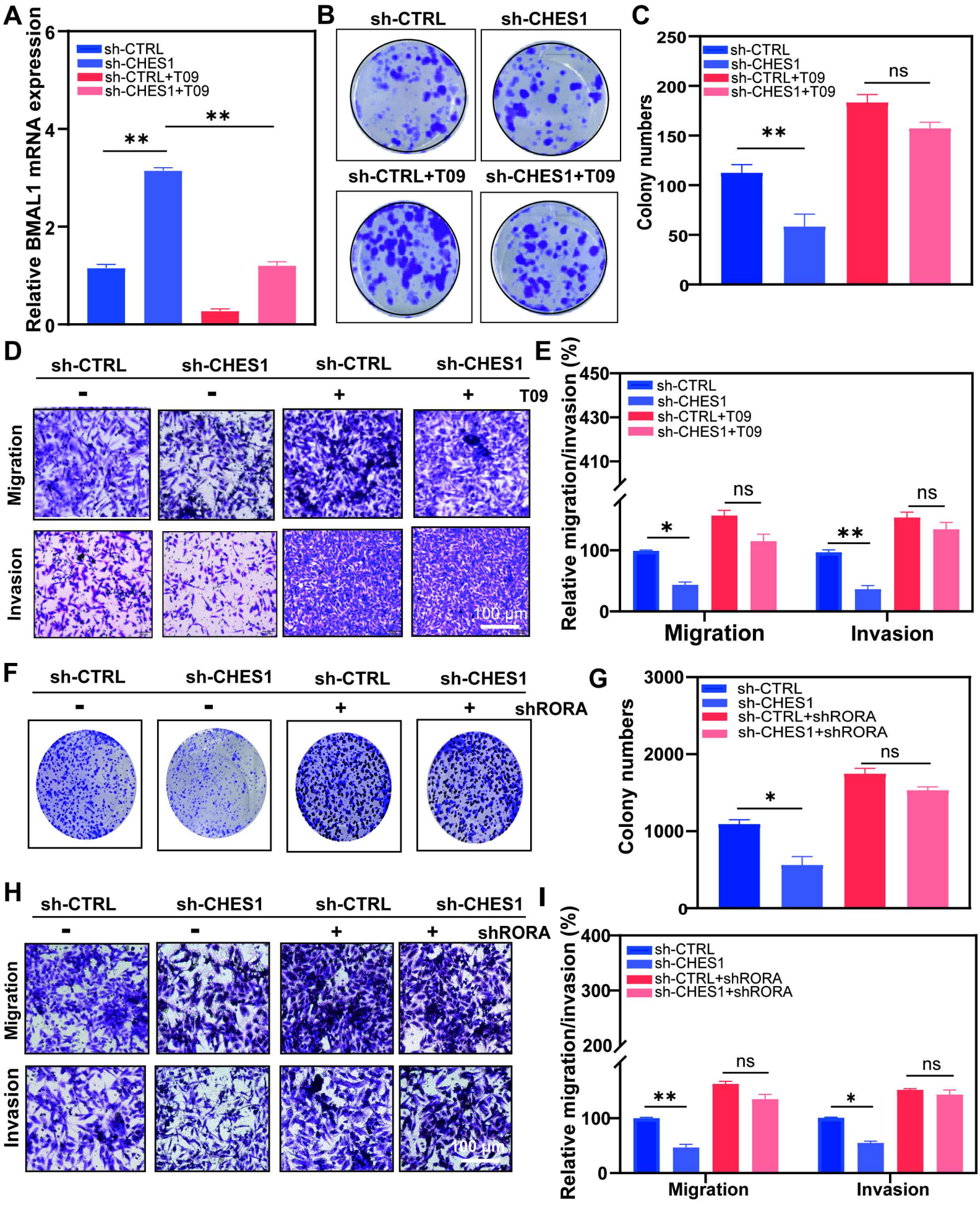
Figure 8. Mechanism diagram: Schematic diagram of the CHES1/RORA signaling axis in TNBC. Nuclear CHES1 directly binds to the promoter of RORA and transcriptionally suppresses RORA expression. RORA functions as a suppressor to block the phosphorylation of PI3K and AKT. Downregulation of RORA elevates p-PI3K and p-AKT levels, consequently facilitating proliferation, migration and invasion of triple-negative breast cancer cells.

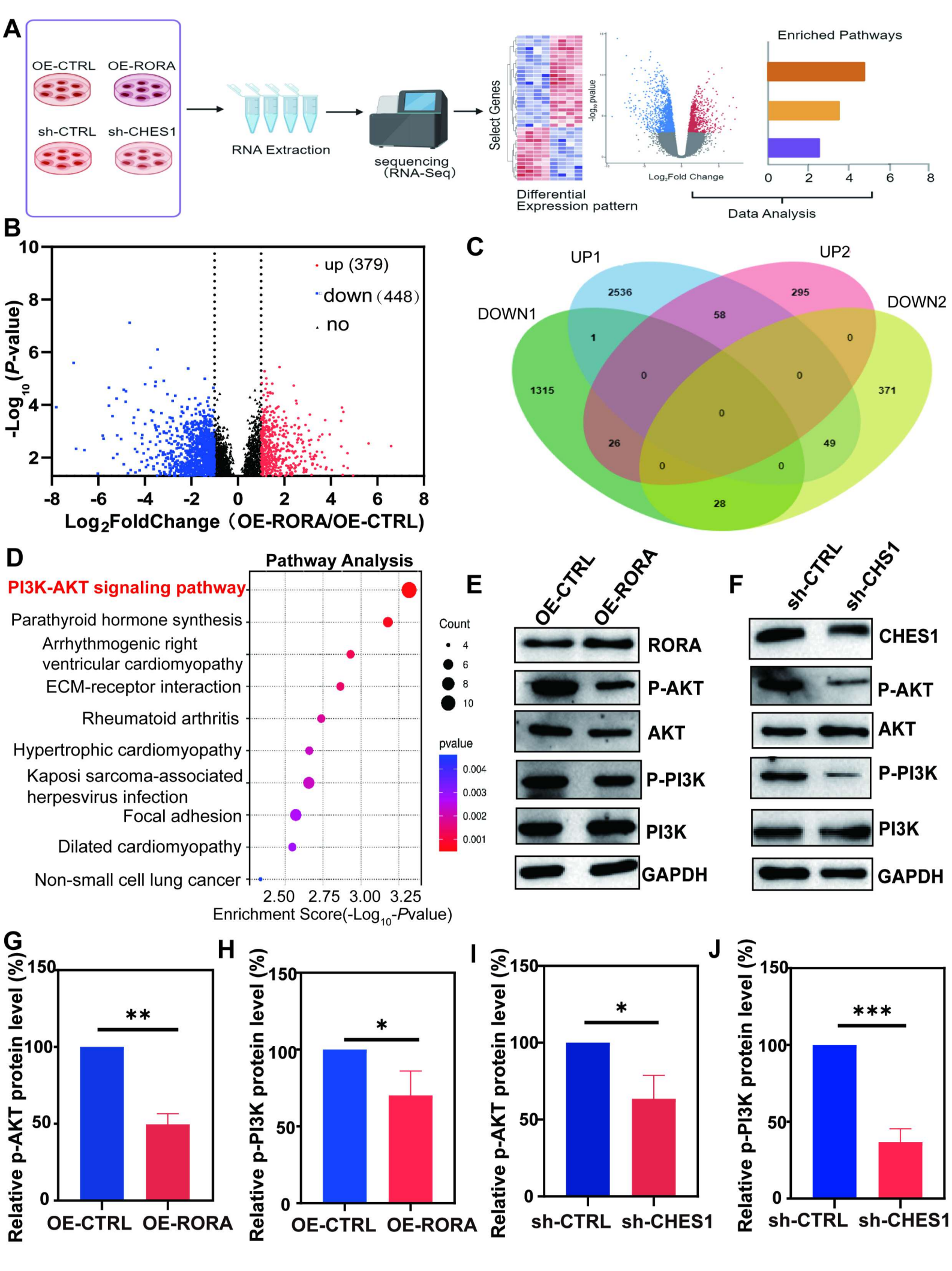

A
MDA-MB-231
sh-CHES1
sh-CTRL
Group
1.5
1
0.5
-0.5
-1
-1.5
B
BT549
sh-CHES1
sh-CTRL
Group
1.5
1
0.5
-0.5
-1
-1.5
C
MDA-MB-231
-Log10(P-value)
Log2(FoldChange)
RORA
D
BT549
-Log10(P-value)
Log2(FoldChange)
RORA
E
RORA in Breast Invasive Carcinoma
Probability of survival (%)
High （n=26）
Low （n=24）
P <0.0001
Years
F
Relative RORA mRNA expression
sh-CTRL
sh-CHES1
***
***
BT549
MDA-MB-231
G
BT549
sh-CTRL
sh-CHES1
CHES1
RORA
GAPDH
H
MDA-MB-231
sh-CTRL
sh-CHES1
CHES1
RORA
GAPDH

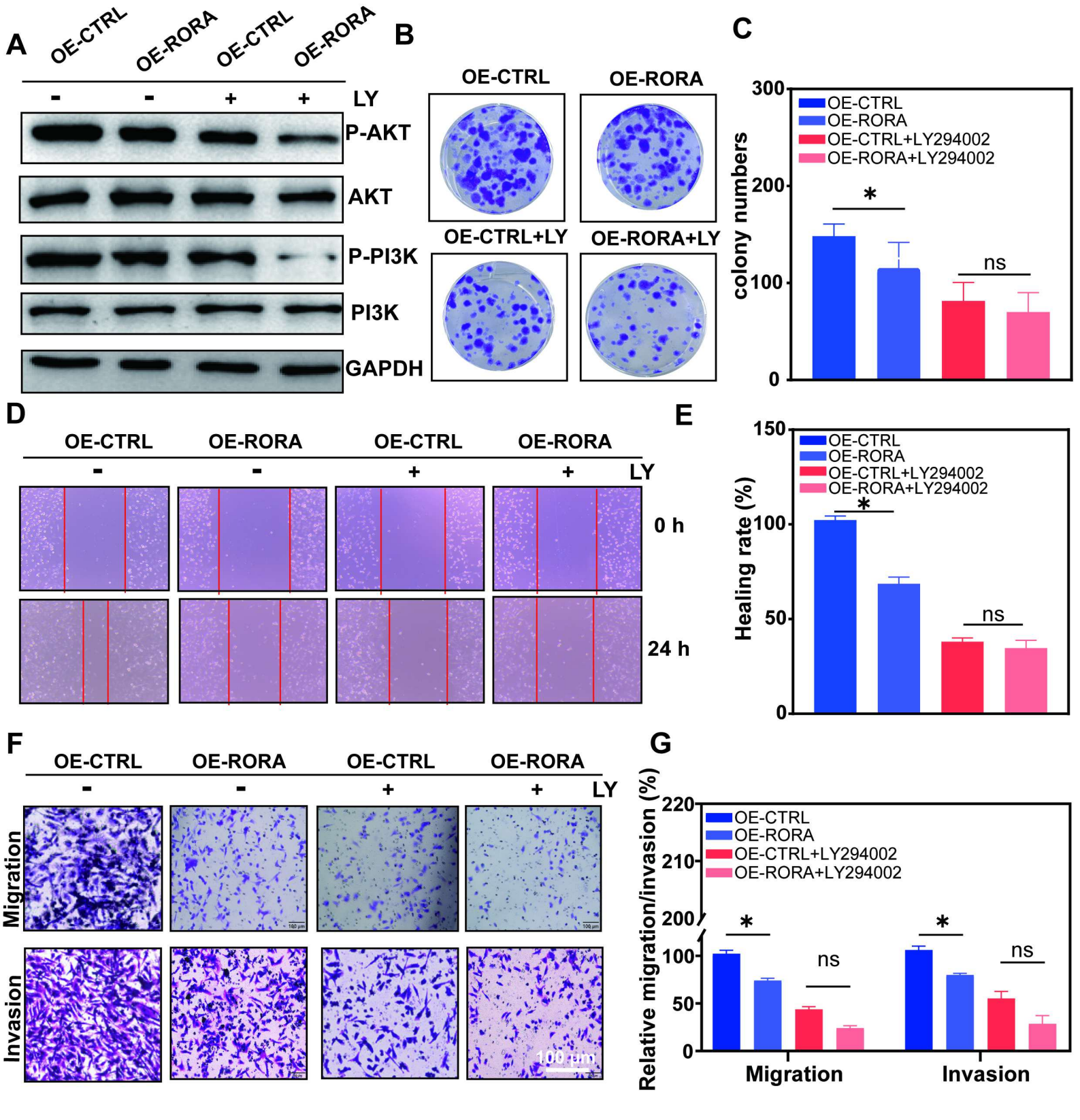


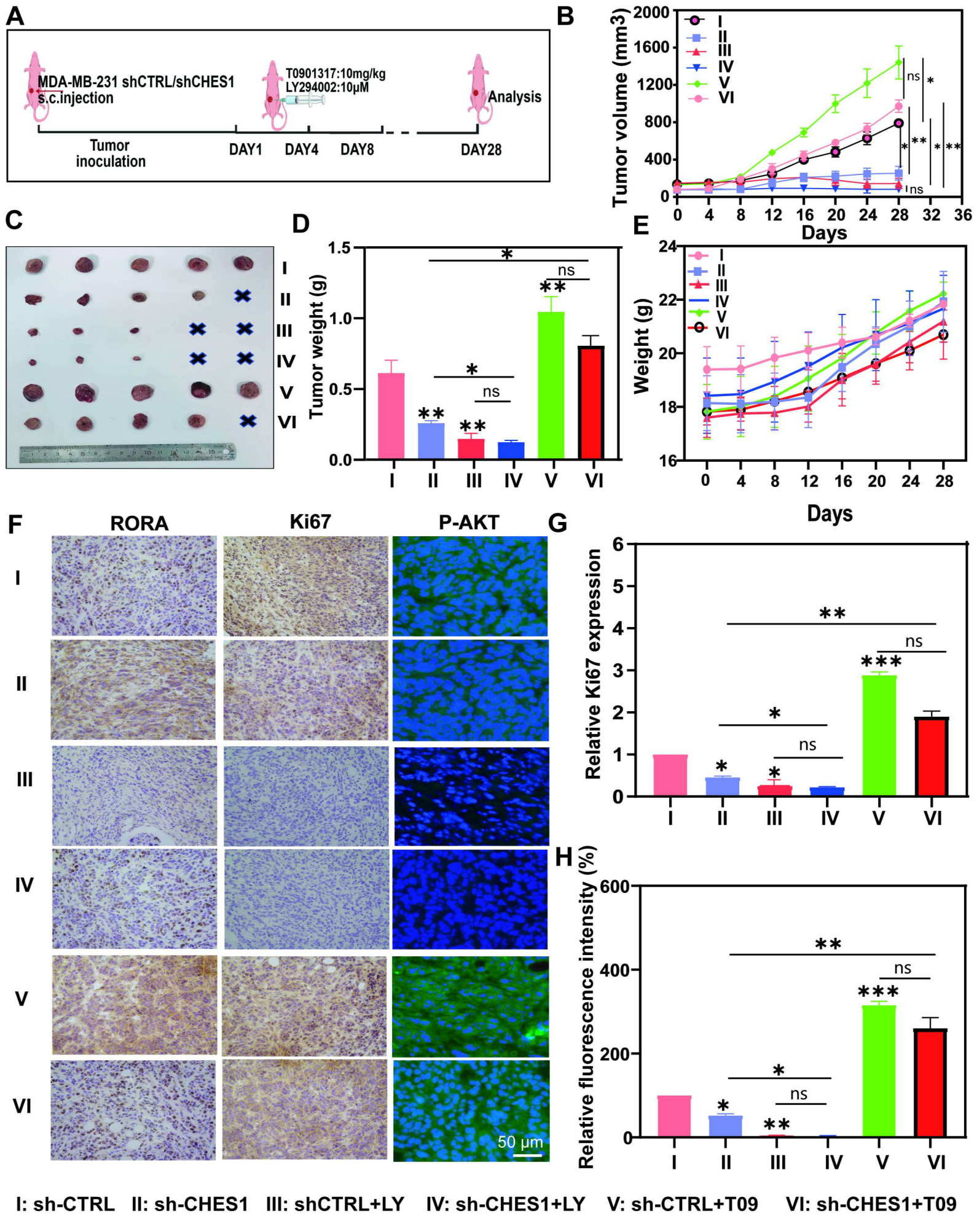
	RORA High	*RORA* Low	total	*P*-value
CHES1 high	1	6	7	
CHES1 low	15	4	19	0.0068
Total	16	10	26	

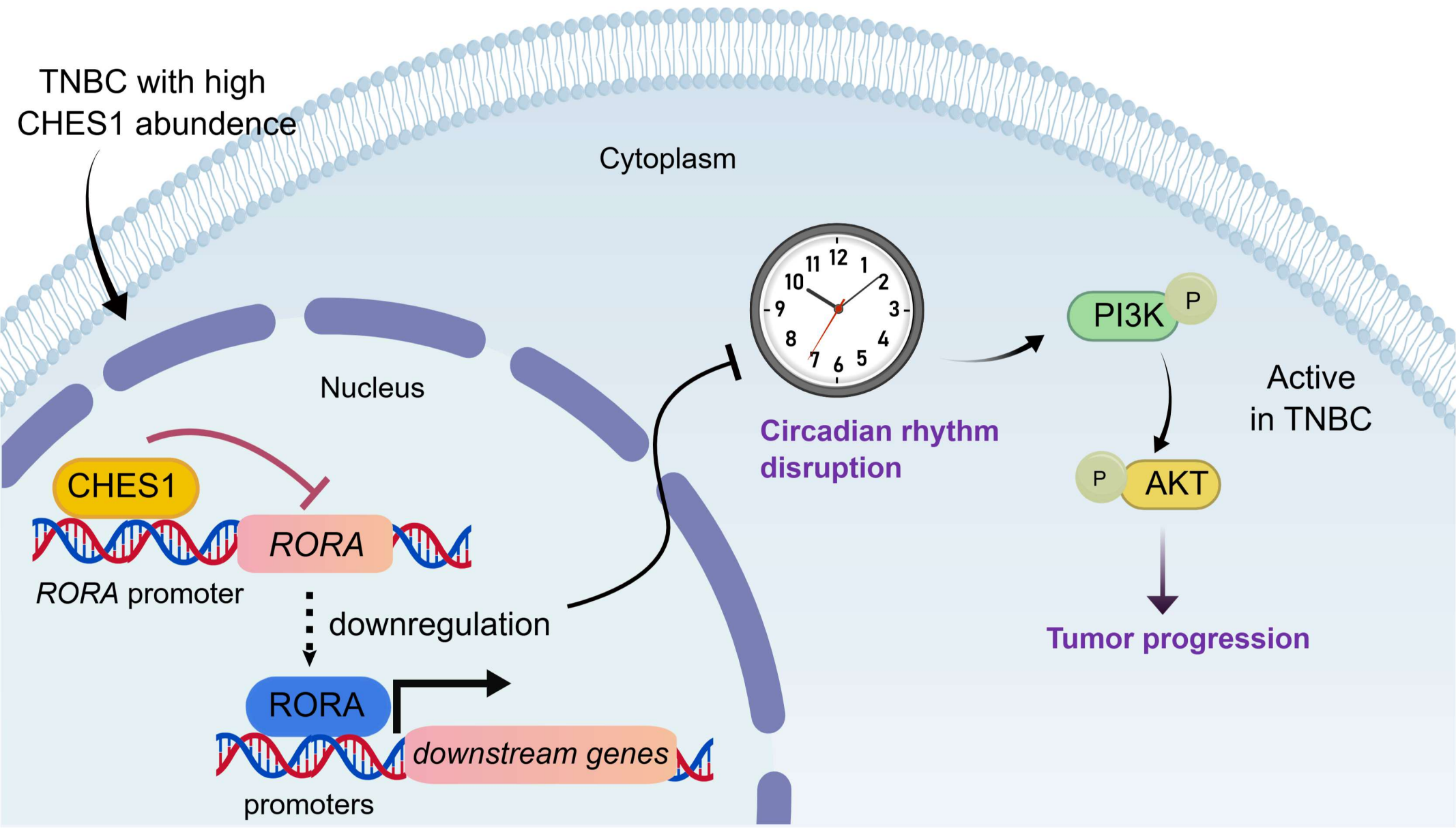

A
OE-CTRL
OE-RORA
RORA
GAPDH
B
OE-CTRL
OE-RORA
Cell viability
Days
***
C
OE-CTRL
OE-RORA
D
Colony numbers
**
OE-CTRL
OE-RORA
E
OE-CTRL
OE-RORA
Migration
Invasion
100 μm
F
Relative migration/invasion (%)
OE-CTRL
OE-RORA
**
**
Migration
Invasion
G
sh-CTRL
sh-RORA
RORA
GAPDH
H
sh-CTRL
sh-RORA
Cell viability
Days
*
I
0 h
24 h
sh-CTRL
sh-RORA
sh-CTRL
sh-RORA
J
Healing rate (%)
sh-CTRL
sh-RORA
**
sh-CTRL
sh-RORA
K
sh-CTRL
sh-RORA
Migration
Invasion
100 μm
L
Relative migration/invasion (%)
sh-CTRL
sh-RORA
**
**
Migration
Invasion


A
Relative BMAL1 mRNA expression
sh-CTRL
sh-CHES1
sh-CTRL+T09
sh-CHES1+T09
**
**
B
sh-CTRL
sh-CHES1
sh-CTRL+T09
sh-CHES1+T09
C
Colony numbers
sh-CTRL
sh-CHES1
sh-CTRL+T09
sh-CHES1+T09
**
ns
D
sh-CTRL
sh-CHES1
sh-CTRL
sh-CHES1
T09
Migration
Invasion
100 μm
E
Relative migration/invasion (%)
sh-CTRL
sh-CHES1
sh-CTRL+T09
sh-CHES1+T09
*
ns
**
ns
Migration
Invasion
F
sh-CTRL
sh-CHES1
sh-CTRL
sh-CHES1
shRORA
G
Colony numbers
sh-CTRL
sh-CHES1
sh-CTRL+shRORA
sh-CHES1+shRORA
*
ns
H
sh-CTRL
sh-CHES1
sh-CTRL
sh-CHES1
shRORA
Migration
Invasion
100 μm
I
Relative migration/invasion (%)
sh-CTRL
sh-CHES1
sh-CTRL+shRORA
sh-CHES1+shRORA
**
ns
*
ns
Migration
Invasion


A
OE-CTRL
OE-RORA
sh-CTRL
sh-CHES1
RNA Extraction
sequencing
(RNA-Seq)
Select Genes
Differential
Expression pattern
Log2Fold Change
Enriched Pathways
Data Analysis
B
up (379)
down (448)
no
-Log10 (P-value)
Log2FoldChange (OE-RORA/OE-CTRL)
C
UP1
UP2
DOWN1
DOWN2
2536
295
58
1
0
1315
371
0
26
49
28
D
Pathway Analysis
PI3K-AKT signaling pathway
Parathyroid hormone synthesis
Arrhythmogenic right ventricular cardiomyopathy
ECM-receptor interaction
Rheumatoid arthritis
Hypertrophic cardiomyopathy
Kaposi sarcoma-associated herpesvirus infection
Focal adhesion
Dilated cardiomyopathy
Non-small cell lung cancer
Count
pvalue
Enrichment Score(-Log10-Pvalue)
E
OE-CTRL
OE-RORA
RORA
P-AKT
AKT
P-PI3K
PI3K
GAPDH
F
sh-CTRL
sh-CHS1
CHES1
P-AKT
AKT
P-PI3K
PI3K
GAPDH
G
Relative p-AKT protein level (%)
OE-CTRL
OE-RORA
H
Relative p-PI3K protein level (%)
OE-CTRL
OE-RORA
I
Relative p-AKT protein level (%)
sh-CTRL
sh-CHES1
J
Relative p-PI3K protein level (%)
sh-CTRL
sh-CHES1


A
OE-CTRL
OE-RORA
OE-CTRL
OE-RORA
LY
P-AKT
AKT
P-PI3K
PI3K
GAPDH
B
OE-CTRL
OE-RORA
OE-CTRL+LY
OE-RORA+LY
C
colony numbers
OE-CTRL
OE-RORA
OE-CTRL+LY294002
OE-RORA+LY294002
ns
D
0 h
24 h
E
Healing rate (%)
F
Migration
Invasion
100 μm
G
Relative migration/invasion (%)
Migration
Invasion


A
MDA-MB-231 shCTRL/shCHES1
s.c.injection
T0901317:10mg/kg
LY294002:10μM
Analysis
Tumor
inoculation
DAY1
DAY4
DAY8
DAY28
B
Tumor volume (mm3)
Days
I
II
III
IV
V
VI
ns
C
D
Tumor weight (g)
E
Weight (g)
F
RORA
Ki67
P-AKT
50 μm
G
Relative Ki67 expression
H
Relative fluorescence intensity (%)
I: sh-CTRL II: sh-CHES1 III: shCTRL+LY IV: sh-CHES1+LY V: sh-CTRL+T09 VI: sh-CHES1+T09


TNBC with high
CHES1 abundence
Cytoplasm
Nucleus
CHES1
RORA
RORA promoter
downregulation
RORA
downstream genes
promoters
Circadian rhythm
disruption
PI3K
P
P
AKT
Active
in TNBC
Tumor progression

Supplementary Files

This is a list of supplementary files associated with this preprint. Click to download.

- Originalwesternblots.pdf
- Supplementaryfigures.pdf
- RTqPCR.xls